NUMERICAL FLUID-STRUCTURE INTERACTION ANALYSIS FOR A FLEXIBLE MARINE PROPELLER USING CO-SIMULATION METHOD

(Reference No: IJME670, DOI No: 10.5750/ijme.v163iA2.759)

A Kumar, R Vijayakumar, **VA Subramanian,** Department of Ocean Engineering, Indian Institute of Technology Madras, India

KEY DATES: Submitted: 31/08/20; Final acceptance: 14/03/21; Published 12/07/21

SUMMARY

Carbon fibre composite has exceptionally high strength, low density and corrosion resistance in the marine environment compared to conventional materials. These characteristics make it a favourable alternative material to be considered for manufacturing marine screw propellers. Despite these advantages, the flexibility of the material leads to a significant change in blade geometry due to loads acting on blades which alter hydrodynamic performance. A two-way coupled fluid-structure interaction analysis is required to accurately capture its hydrodynamic performance due to the reduced stiffness and material anisotropy. The present study focuses on numerical investigation for the hydro-elastic based performance analysis of a composite marine propeller in open water condition. The procedure involves the coupling of Reynolds-Averaged Navier-Stokes Equation based computational fluid dynamics solver with the finite element method solver using co-simulation technique. The open water characteristics, including thrust coefficient, torque coefficient and open water efficiency, are discussed as a function of advance ratio. This paper presents a comparison of the hydrodynamic performance and structural responses between a carbon fibre composite propeller and a conventional steel propeller which are geometrically identical. The results for the composite propeller show a significant improvement in hydrodynamic performance compared to the metallic propeller while remaining structurally safe throughout the tested range.

NOMENCLATURE

C	Chord length (m)
D	Blade diameter (m)
E	Young's modulus (N/m^2)
G	Rigidity modulus (N/m^2)
J	Advance ratio
n	Revolution per second
N	Revolution per minute
r	Propeller radius (m)
Z	No of blades
K_T	Thrust coefficient
K_Q	Torque coefficient
p	Pressure (N/m^2)
V_a	Advance velocity (m/s)
V_r	Resultant velocity (m/s)
Δt	Time step (s)
α	Angle of attack
β	Inflow angle
η_o	Open water efficiency
μ	Dynamic viscosity (N.s/m^2)
ρ_f	Density of fluid (kg/m^3)
ρ_s	Density of solid (kg/m^3)
υ	Poisson ratio
ϕ	Pitch angle
BEM	Boundary Element Method
CFD	Computational Fluid Dynamics
FEM	Finite Element Method
FSI	Fluid-Structure Interaction
FVM	Finite Volume Method
LES	Large Eddy Simulation
RANSE	Reynolds-Averaged Navier-Stokes Equation

1. INTRODUCTION

Marine propellers are hydrodynamic rotating components designed to deliver thrust to overcome resistance. Typically, they are rigid and have a fixed geometry. Over the past few decades, the propellers have been optimised to their maximum performance limit. Some of the conventional materials used for manufacturing marine propellers are manganese-bronze, nickel-aluminium-bronze, aluminium, and steel. They were well proven to deliver the thrust efficiently; however, they exhibit some unfavourable characteristics such as relatively moderate specific strength (strength to weight ratio), fewer fatigue cycles, susceptibility to cavitation, corrosion and relatively more prone to noise and vibration. Therefore, it is worth considering the composite materials as an alternative to conventional materials for manufacturing marine propellers. It comes with numerous advantages such as high specific strength, improved fatigue cycles and enhanced acoustic properties.

The conventional propellers are evaluated for hydrodynamic performance by performing different tests: open water test, self-propulsion test and cavitation test. These tests are typically carried out based on rigid body assumptions for propellers made of conventional materials. For composite marine propellers, which have lower flexural rigidity, the effect of structural deformation on hydrodynamic aspects and vice-versa must be taken into account while determining its hydrodynamic performance. The deformation influences the propeller hydrodynamic performance by changing the blade angle of attack. The propellers are also subjected to highly unsteady forces due to the heterogeneous nature of hull's wake, which adds to the existing physical complexities. Hence, it is worthwhile to perform a two-way FSI analysis to assess the hydrodynamic performance and structural responses of the propeller.

Mouritz *et al*. (2001) said experimental studies on composite propellers began in the early 1960s for a Soviet fishing craft where full-scale propellers up to 2m diameter were tested for performance and continued up to 6m diameter propellers in the early 1970s. Young *et al.*(2017) explained that due to recent developments in computational techniques, several potential flow-based solvers (boundary element method, lifting line method) could be coupled with the structural solver to perform inviscid FSI analysis of propeller hydrodynamic performance. Lin and Lin (1996) studied the hydro-elastic based analysis by coupling lifting surface theory and finite element method on a flexible propeller. Lin (2005) explained the structural performance of the composite blade by nonlinear hydro-elastic analysis, and the effect of the fibre stacking sequence on propeller performance was considered along with failure modes. In the late 2000s, Young (2007, 2008) studied composite propeller performance in uniform and wake flow using the BEM coupled with FEM. It was reported that the possibility of hydro-elastic tailoring of propeller blade geometry improves their hydrodynamic performance. Although the potential flow methods discussed above are relatively less complicated and give fairly accurate quicker results than higher fidelity methods, it is essential to consider the viscous effects because the propeller always operates in the viscous regime. The presence of the ship's wake adds to the already existing complexities. As several viscous models available to solve complex problems, RANSE, LES, and hybrid RANSE-LES are popular. Among these, RANSE, generally based on the FVM considered computationally cheap and effective to obtain a fairly accurate solution.

Some RANSE based works include design and optimisation of the flexible propeller to tailor the flexible laminate to control the deformation shape and subsequently improve the thrust by Blasques *et al*. (2010). Ducoin and Young (2013) investigated the hydroelastic response and stability of hydrofoil using commercial CFD solver focusing on viscous effects such as, laminar to turbulent transition as well as stall and validated the same with experiments. Akcabay and Young (2013) numerically examined 2-D rectangular hydrofoil to identify the effect of turbulent and cavitating flow. The fluid flow was modelled with the incompressible, URANSE equations using an eddy-viscosity turbulence closure and with transport equation based cavitation model. Ghassabzadeh *et al*. (2013) and Han *et al.* (2015) adopted the FVM-FEM coupling procedure to investigate the flexible propeller. Garg *et al.* (2015) developed a CFD based hydrodynamic shape optimisation tool for 3D hydrofoils considering cavitation and wide range of operating conditions. The study considered as many as 210 design variables to obtain an optimal solution. The above numerical tool was validated in Garg *et al.* (2018). Young *et al.* (2018) studied the steady-state hydroelastic response of composite hydrofoils considering the loads mainly from bend-twist coupling effects.

Maljaars *et al*. (2018) performed experimental studies on the composite propeller to analyse the performance and validated BEM and RANSE with FEM coupling methods. Liao *et al.* (2018) studied the influence of fibre orientation on the vibration characteristics and load-dependent bend-twist coupled behaviour of composite hydrofoils made of carbon fibre in viscous flow. Kumar *et al*. (2018) & Kumar *et al.* (2019) conducted open water studies on two propellers having identical geometry manufactured using carbon fibre composite as well as homogeneous isotropic metal. It has been observed that the composite propeller delivered better hydrodynamic efficiency than the metal propeller. Both the propellers were also subjected to structural analysis where tip deflection was measured using static loading test and FEM. The two-way FSI analysis is a vital step involved in designing a carbon fibre composite propeller in pursuit of its favourable material properties and better hydrodynamic performance compared to conventional marine propellers while keeping the structural deformations within the safe limit.

The objective of the current work is to establish a two-way fluid-structure interaction method for composite marine propeller by using the RANSE solver to compute the hydrodynamic performance and the FEM solver for the structural response. Two geometrically identical propellers, one made of steel and another made of carbon fibre were designed based on the standard series diagram method to operate at advance ratio (J) of 0.5. Due to ease of availability of material and also to include the rigid properties, steel propeller was considered instead of nickel aluminium bronze, as the current study is a prequel for the experimental analysis.

The geometry was unaltered during manufacturing at static condition. The RANSE based commercial CFD solver StarCCM+ was coupled with FEM based commercial structural solver ABAQUS to perform FSI simulation using co-simulation technique. The propeller performance was analysed in open water condition both with and without coupling and was compared with regression series data. The blade tip deflection and stresses obtained for both the materials were compared.

2. NUMERICAL MODELING APPROACH

This section explains the different steps involved in performing FSI analysis of propeller, starting from the design and development of propeller, setting up fluid & solid model and FSI interface. The grid sensitivity is also briefly discussed.

2.1 MODEL PREPARATION USING CAD

The propeller parameters derived from a candidate hull (Oil tanker) form using appropriate hull-propeller interaction components. It was developed using the standard series by Troost (1938, 1940, 1951) that extensively used for the propeller design. The design also incorporates the Reynolds correction suggested by Oosterveld (1969); Oosterveld and van Oossanen (1975). The propeller with a diameter (D) of 1.785m; the number of blades (Z) as 4; Pitch to diameter ratio as 0.826; rake angle as 15°.

The radial sections are generated using empirical relations and wrapped over the cylindrical surface. The final propeller blade geometry developed using a 3-D CAD software Rhinoceros. Figure 1 shows the front and side view of propeller CAD geometry.

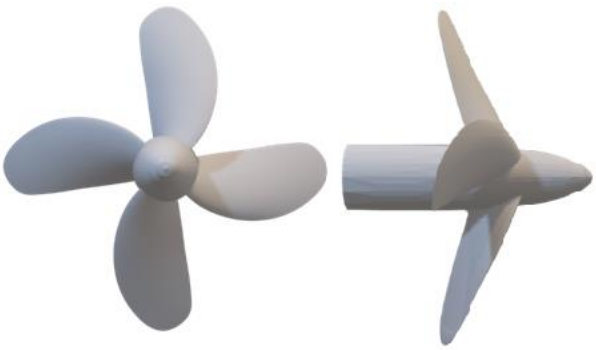

Figure 1: Front and side views of the propeller

2.2 FLUID MODEL

The governing equation, i.e., continuity and Reynolds Averaged Navier-Stokes Equation is solved inside the computational domain using StarCCM+. The fluid is water, and hence the flow is assumed to be incompressible. The flow is unsteady and turbulent condition are applicable.

$$\frac{\partial \rho}{\partial t} + \nabla.(\rho U) = 0 \tag{1}$$

$$\frac{\partial \rho U}{\partial t} + U.\nabla U = -\nabla p + \mu \nabla^2 U + \rho g \tag{2}$$

Where ρ_f is the fluid density, U is the velocity with x, y and z components as u, v & w, p is pressure, μ is dynamic viscosity, and t is time. Finite volume discretisation method used for solving the governing equation inside the computational domain. The computational domain is a cylindrical quadrant with length 16 D and diameter 7 D with propeller located at 4 D from the inlet. Due to the periodicity of the problem, only a quadrant solved using the periodic boundary condition. It makes the simulation computationally tractable. Figure 2 shows the computational domain in with boundary conditions.

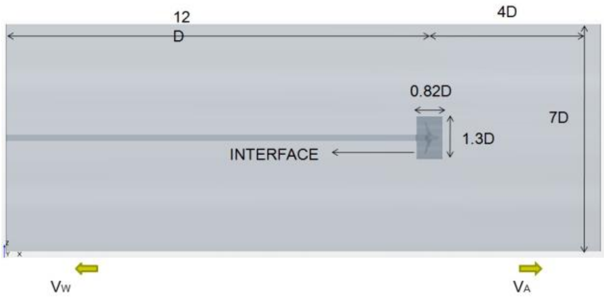

Figure 2: Computational domain for fluid analysis

The computational domain consists of two regions, namely a stationary region and a rotating inner region which consist of the propeller. The rotating inner region is also a cylindrical quadrant of length 0.82 D and diameter 1.3 D with the propeller at the centre. The domain size was decided as per ITTC recommendation 75-03-03-0 and also with the literature [11,19]. The two regions are connected by a non-conformal fluid-fluid interface to transfer the flow quantities. The interface boundaries of two connected regions are not separated in space. Moving Reference Frame (MRF) method with periodic boundaries was adopted for the study. k-ε turbulence model is considered with two-layer wall y+ treatment. Wall Y+ value used in the study is 50.

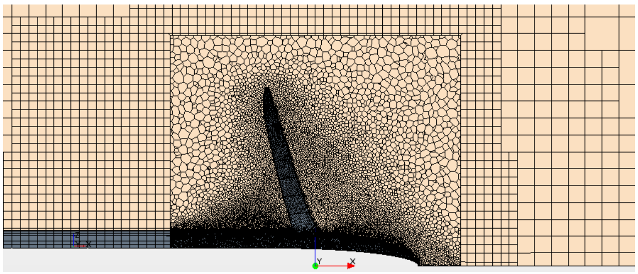

(a) Fluid mesh

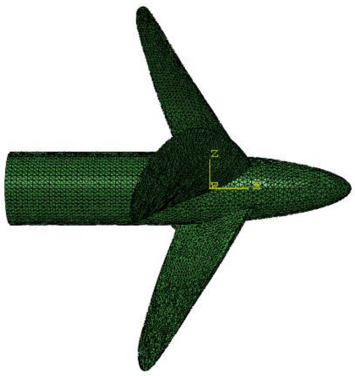

(b) Solid mesh

Figure 3: Mesh for fluid model (a) & solid model (b)

Hexahedral cells were used to mesh the stationary outer region, while polyhedral cells were used to mesh the rotating inner region. The boundary layer on the propeller blades and the hub were captured with six prism layers with near-wall height 6.8×10^{-5} m with a growth rate of 1.2. The cell size grows gradually from the propeller. The mesh used for the fluid model is shown in Figure 3 (a).

The simulation was performed for the full-scale propeller for different advance ratios with the propeller rotating at a constant 286 rpm. Water density (1025 kg/m^3) and dynamic viscosity (8.88×10^{-4} Pa.s) were given as input to the solver. Inlet velocity (operating condition) is 4.25 m/s (J = 0.5).

Figure 4 shows the blade velocity diagram for a radial section (0.7r) for composite propeller at the operating condition where Δα represents the improved angle of attack.

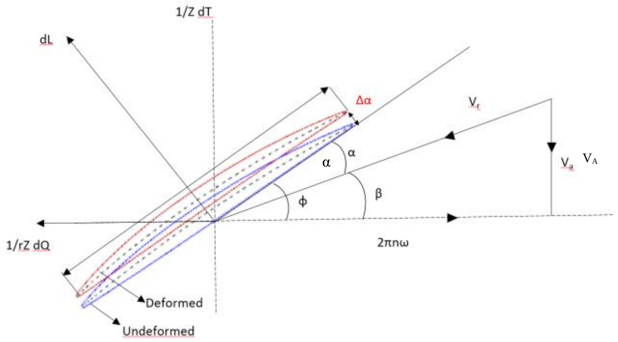

Figure 4 Blade velocity diagram

2.3 SOLID MODEL

The general equation of the motion for the propeller blade in the solid model is defined as follows.

$$a\ddot{x} + b\dot{x} + cx = F_T \tag{3}$$

Where, a is the mass matrix, b is damping matrix, c is stiffness matrix, $\ddot{x}$ is acceleration, $\dot{x}$ is velocity, and x is displacement. F_T is the total external force. The structural behaviour of the propeller was computed by FEM using commercial solver ABAQUS. Both the steel and the composite propellers modelled in the solid solver. Steel propeller modelled as a homogeneous isotropic material. Whereas carbon fibre modelled as an anisotropic material by specifying the fibre direction.

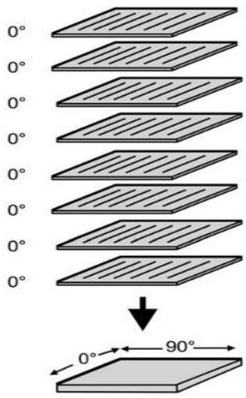

.

Figure 5 Stacking sequence in unidirectional style

Since this is a preliminary study on the composite propeller, the fibre directions kept as unidirectional throughout the thickness and same is shown in Figure 5. Due to the complexity of the blade geometry, unstructured tetrahedral elements were used for the solid model. A minimum of three elements across the blade trailing edge was used. The mesh used for the solid model is shown in Figure 3 (b).

The material properties of the steel and carbon fibre are given in Table 1 (a) and (b) respectively. The root of propeller blades treated as fixed boundaries.

Table 1: Material properties of steel (a)

Description	Value
Density (ρ_s)	7850 kg/m^3
Poison ratio (υ)	0.3
Young's modulus (E)	210 GPa
Yield strength (σ_y)	450 MPa

Material properties of carbon fibre (b)

Description	Value
Density (ρ_s)	1600 kg/m^3
Young's modulus (E_{11})	149 GPa
Young's modulus (E_{22})	8.33 GPa
Young's modulus (E_{33})	8.33 GPa
Poison ratio (υ_{12})	0.342
Poison ratio (υ_{13})	0.342
Poison ratio (υ_{23})	0.35
Rigidity Modulus (G_{12})	5.38 GPa
Rigidity Modulus (G_{13})	5.38 GPa
Rigidity Modulus (G_{23})	2.98 GPa
Ultimate strength (σ_y)	2400 MPa

2.4 SOLID-FLUID INTERFACE

In the fluid model, FSI interface was created at propeller surfaces which takes displacement as input from the solid solver and gives the hydrodynamic forces (pressure + shear) to the solid solver. The interface mesh surfaces will deform according to the displacement. Morpher model was used to control the deforming mesh in the inner rotating region according to the displacement at the interface. The neighbouring cells based on Radial Basis Function (RBF) are displaced in a smoothened manner while maintaining a pre-specified grid density (thin-out factor) in the morpher model. At the new location of mesh vertices, all field data are updated based on interpolation to determine the flow solution at the next time step. The solved pressure and shear force on the interface are exported to the solid model.

Likewise, in the solid model, another FSI interface was created at the propeller surface, which takes the pressure and shear forces from the fluid model as input to compute displacements and stresses. A constant Δt maintained for both fluid and solid solvers. However, ABAQUS will automatically adjust step increment in order to maintain numerical stability.

Interpolation is used at both interfaces before and after data transfer since the mesh interfaces are non-conformal (fluid and solid solvers use different types of meshes). It must also be ensured that the common surface (propeller) in both solvers must be spatially identical in order to enable accurate data transfer between solvers. This surface requires a finer than usual mesh on both solvers to capture high curvature as well as to ensure smooth interpolation of field data.

2.5 GRID INDEPENDENCE STUDY

Grid independent study was carried out with three different grids for fluid solver: coarse (0.8 million), medium (1.18 million) and fine (1.8 million). Sufficiently fine grid (0.3 million elements) was used for the solid model, and hence it was kept unchanged for the study. Figure 6 shows the grid independence study for three different mesh values with corresponding K_T and K_Q. Medium grid was chosen for the present study since the thrust difference between medium and fine was less than 1% for both steel and carbon fibre propellers.

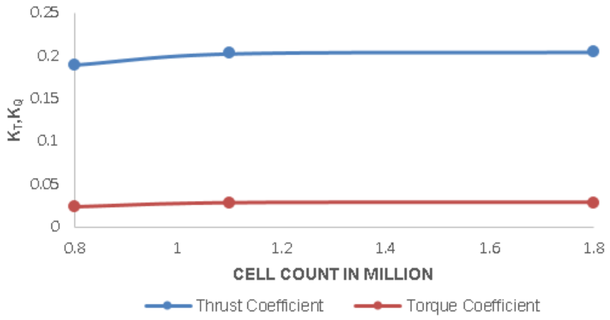

Figure 6: Grid Independence study

3. FLUID STRUCTURE INTERACTION

The independent fluid solver (StarCCM+) and structural solver (Abaqus) are connected by an inbuilt co-simulation engine in StarCCM+. Figure 7 shows the block diagram of FSI coupling mechanism. There are two coupling schemes available, explicit and implicit coupling scheme. The explicit scheme is used for applications with weak coupling between the structure, and the fluid, i.e., the effect of the fluid on the structure is negligible compared to the effect of the structure on the fluid. At the same time, the implicit coupling scheme is used when the coupling between structure and fluid is strong. In implicit coupling, data exchange happens more than once per timestep.

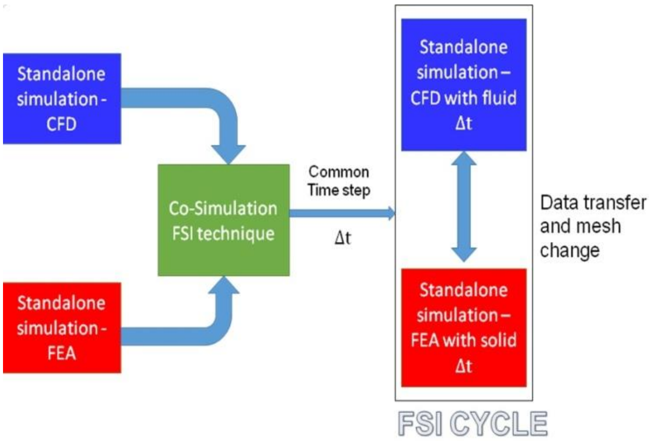

Figure 7: FSI coupling mechanism

Serial coupling scheme was used in the present study where, the fluid solver leads the solid solver and solves the flow to a pre-set target time, while the solid solver waits. At the rendezvous time, the solved flow data (pressure and shear forces) are passed to the solid solver, which then advances to the target time, while the fluid solver waits. After the solid solver is also marched to the rendezvous time, the solved solid data (displacement) are passed to the fluid solver. Figure 8 illustrates the serial coupling method.

In step 1, fluid solver initiates and solves for flow variables for a given time step, Δt and hydrodynamic forces are determined. In Step 2, these hydrodynamic forces are transferred from fluid solver to solid solver while fluid solver waits. These forces are applied to the structural model, and the deformation and stresses are solved by structural solver in Step 3. In Step 4, these deformations are transferred from solid solver to the fluid solver. Step 1 to 4 repeats to form “FSI cycle” which constitutes one coupling step. At the end of each coupling step, the solution quantities are up to date. The solution is marched till steady state is reached. In the present study, the timestep for both solvers and coupling timestep was maintained constant, which is 0.01s. Total no of iteration used to achieve steady-state is around 8500 for steel and 13000 for the composite propeller. Total timestep (coupling) for steel is 750 and for the composite is 1782.

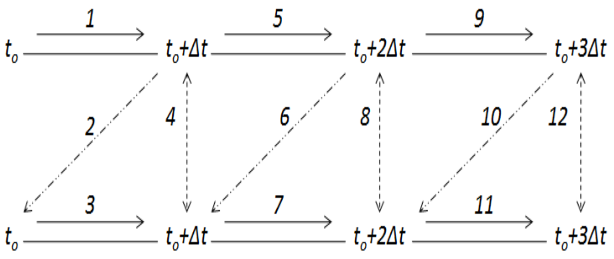

Figure 8: Flowchart for the serial coupling method

4. RESULTS AND DISCUSSION

The hydrodynamic performance parameters of the propeller geometry such as thrust coefficient (K_T), torque coefficient (K_Q) and open water efficiency (η_o) were obtained for various advance coefficient (J) using CFD simulation without considering the solid model (without FSI coupling). This performed as a part of validating the CFD results using regression curves of experimental data from the literature (Oosterveld and van Oossanen 1975). It shows that the numerical results have a good agreement with the regression curves from literature, and the difference was found to be less than 4%. This method indicates good validation of CFD simulation and, hence it is suitable for performing FSI analysis where the material properties considered.

The hydro-elastic based performance analysis was computed for two different propeller materials using co-simulation technique. The open water hydrodynamic performance results of steel propeller and carbon fibre propeller are presented in Figure 9, along with regression curves from literature. It was identified that the thrust and torque coefficient has increased by 3.25% and 5.51% for carbon fibre composite propeller compared to steel propeller at operating condition (J = 0.5). This increase in thrust coefficient increases with decrease in J. At the bollard pull condition (J = 0), the carbon fibre propeller produces 28.08% thrust and 34.24% torque than steel propeller. Hence it is clear that carbon fibre propeller outperforms in thrust production throughout the operating range (J = 0 to 0.5).

All simulations were run for sufficiently long simulation time such that the monitored propeller tip deflection achieves steady-state response. The defection magnitude contours of steel and carbon fibre propellers operating at J = 0.5 are shown in Figure 10. Both the propellers experience predominantly bending deflection along the positive x-direction, which can also be clearly observed from Figure 11, which shows the deformed and undeformed shapes of the composite propeller operating at J = 0.5. It is observed from Figure 10 that the defection at the blade tip is maximum for both propellers, which is 2.16 mm and 55.80 for steel propeller and carbon fibre propeller respectively. The tip deflection of carbon composite propeller is around 26 times as that of the steel propeller. Unlike steel propeller, the composite propeller shows a significantly large defection due to the reduced stiffness.

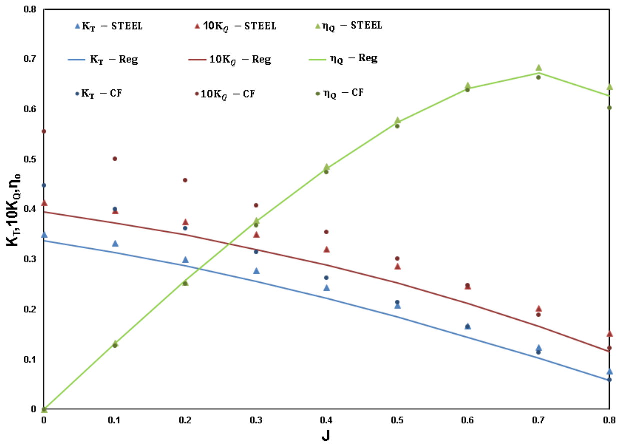

Figure 9: Hydrodynamic performance curves in open water condition for steel and carbon fibre propeller

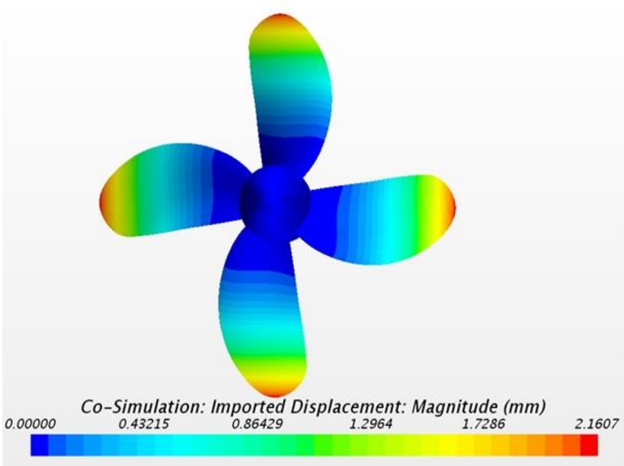

(a) Steel propeller

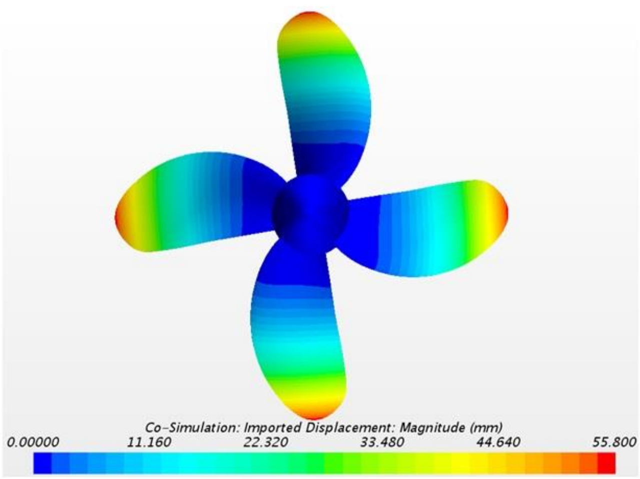

(b) Carbon fibre composite propeller

Figure 10: Contours of defection magnitude of steel and carbon fibre propellers at J = 0.5

From Figure 11, it can be seen that the deformation of carbon composite propeller has caused a notable change in overall propeller blade geometry at J = 0.5. These geometric changes due to hydrodynamic loading include (a) reduction in effective rake angle at the tip by 22.5% from initial rake angle of 15° to 11.62° (b) change in position of chord section along the radius. As a result, the deformed propeller blade has an increase in the effective angle of attack, which enhances thrust production compared to steel propeller, which is practically same as the undeformed propeller. This is in line with the observations made at J = 0.5 from Figure 9. The reduction in rake angle also causes an increase in effective blade diameter by 1.68%.

Figure 12 shows the blade tip defection of both carbon fibre and steel propellers for the tested range advance ratio. It shows that the tip deflection is more for carbon fibre propeller than steel at all advance ratios.

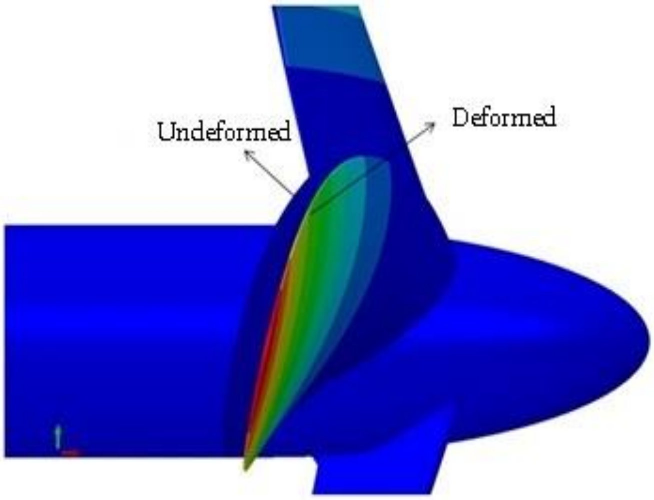

Figure 11: Undeformed and deformed geometry of carbon fibre composite propeller at J = 0.5

The maximum tip deflection occurs at bollard pull condition for both propellers due to higher hydrodynamic load experienced by the propellers. The mechanism of large tip deflection, causing an increase in the local angle of attack, which leads to improved thrust coefficient as observed in Figure 11 (J = 0.5) occurs at all advance ratios. The deflection as a percentage of blade root to tip length found to be 0.29% for the steel propeller and 7.60% the composite propeller.

Though the composite propeller shows better hydrodynamic performance, it must be structurally safe for the entire range of operation. Figure 13 shows the von Mises stress on both the steel and carbon fibre propeller at the operating condition. It was observed that the maximum stresses which occur at blade root for steel and carbon fibre found to be 59.5 MPa and 98.96 MPa respectively. The above stress values for both propellers found to be several orders less than their corresponding yield stresses given in Table 1. It has been also noticed the stresses distribution along the radius appears to be more concentrated at the root for steel propeller while the distribution is more even for the composite propeller.

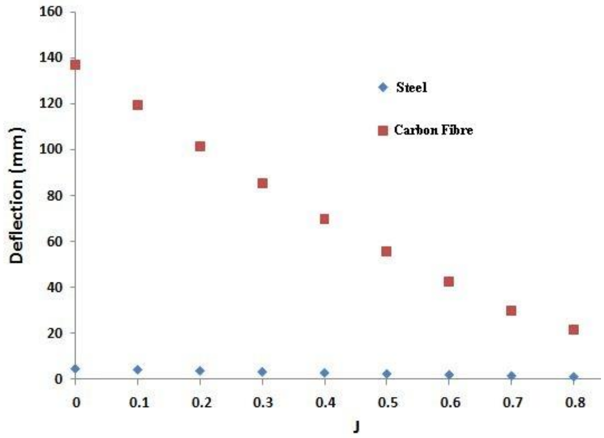

Figure 12: Blade tip defection for steel and carbon fibre propeller

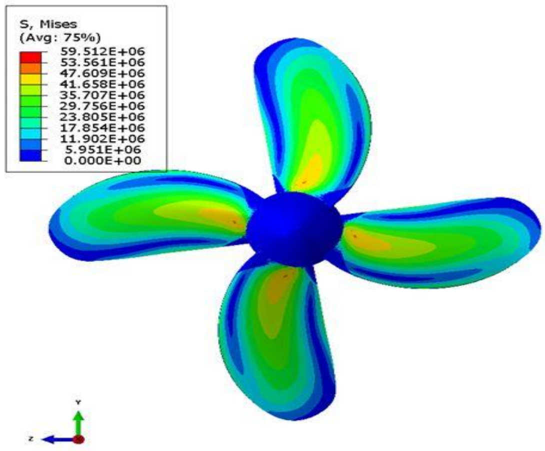

(a) Steel propeller

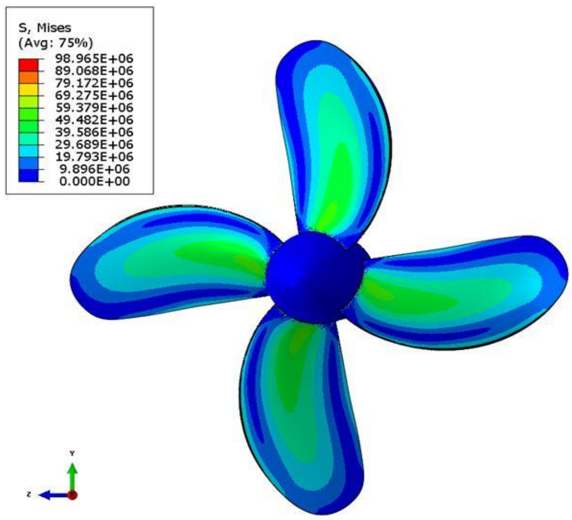

(b) Carbon fibre propeller

Figure 13: von Mises stress distribution at operating condition (J=0.5)

5. SUMMARY AND CONCLUSION

The hydro-elastic based performance analysis was conducted for steel and carbon fibre composite propeller having identical geometry in open water condition using co-simulation method. The RANSE based CFD solver was coupled with the FEM solver, and data exchange was based on serial coupling method. The following conclusions were drawn from the study.

- The open water results of the coupled analysis were also compared and found that the carbon composite propeller delivers better hydrodynamic thrust than the conventional metal propeller.
- The thrust and torque coefficient was found to increase up to 3.25% and 5.51%at the operating condition for the carbon composite propeller compared to steel propeller.
- At operating condition, the blade tip defection is 2.16 mm for steel propeller whereas it is 55.8 mm for carbon composite propeller.
- The deflection causes a reduction in rake angle by 22.5%, and it also increases effective blade diameter by 1.68 %.
- Von Mises stress was obtained using FEM solver and found to be 59.5 MPa for steel propeller and 98.96 MPa carbon composite propeller. These stress values are well below the yielding/breaking limit.
- The hydro-elastic methodology adopted in this study was found to be efficacious in determining the hydrodynamic performance as well as the structural behaviour of a composite propeller.
- As the composite materials are lesser rigid, the propeller blade sections and geometery shall be optimised using the above methodology. It allows to tailor the blade profile to achieve the maximum thrust and efficiency.

6. REFERENCES

1. ABAQUS, 2014. Version 6.14 User's Manual, Dassault Systèmes Simulia Corp.; Providence, RI, USA.
2. AKCABAY D.T, YOUNG, Y.L.2013 *Understanding and Toward Controlling the Hydroelastic Response and Stability of Hydrofoils in Cavitating Flows,* 66th annual meeting of APS Division of Fluid Dynamics 58, Pennsylvania, USA
3. BLASQUES, J.P., BERGGREEN, C., ANDERSEN, P. 2010. *Hydro-elastic analysis and optimisation of a composite marine propeller*. Marine Structures 23, 22–38.DOI: 10.1016/j.marstruc.2009.10.002
4. CD-ADAPCO 2012. *User guide, STAR-CCM+*. Star-CCM+.
5. DUCOIN, A., YOUNG, Y.L. 2013. *Hydroelastic response and stability of a hydrofoil in viscous flow* Journal of Fluids and Structures 38, pp 40-57.
6. GHASSABZADEH, M., GHASSEMI, H., & SARYAZDI M.G., 2013. *Determination of hydrodynamics characteristics of marine propeller using hydro-elastic analysis.* Brodogradnja 64, pp 40–45.
7. GARG,N, LYU, Z, DHERT, T, MARTINS, J, YOUNG, Y.L, 2015. *High-fidelity Hydrodynamic Shape Optimization of a 3-D Morphing Hydrofoil*. Fourth International Symposium on Marine Propulsors. SMP'15. Texas, USA 59.
8. GARG, N., PEARCE, B.W, BRANDNER. A.P., PHILLIPS A.W., MARTINS, R.R.A. J. YOUNG, Y.L. 2018. *Experimental investigation of a hydrofoil designed via hydro structural optimisation,* Journal of Fluids and Structures 84, 243-262. DOI: 10.1016/j.jfluidstructs.2018.10.010
9. KUMAR, A., LAL KRISHNA, G., & SUBRAMANIAN, V.A. 2018. *Design and analysis of a carbon composite propeller for podded propulsion.* 4th International Conference on Ocean Engineering. Springer, Chennai, pp. 203–215.DOI:10.1007/978-981-13-3119-0_13.
10. KUMAR, A., SUBRAMANIAN, V.A., AND VIJAYAKUMAR, R. 2019. *Hydro-elastic analysis of carbon composite marine propeller using co-simulation technique.* International Conference in Marine Engineering and Technology. ImarSET, Muscat.
11. KUMAR, J., AND WURM, F.-H. 2015. *Bi-directional fluid–structure interaction for large deformation of layered composite propeller blades.* Journal of Fluids and Structures 57, 32–48. DOI: 10.1016/j.jfluidstructs.2015.04.007.
12. LIAO, Y., GARG, N., MARTINS, R.R.A. J. YOUNG, Y.L. 2018. *Viscous fluid–structure interaction response of composite hydrofoils,* Composite Structures 212, pp 571-585. DOI: 10.1016/j.compstruct.2019.01.043
13. LIN, H.J. 2005. *Strength Evaluation of a Composite Marine Propeller Blade*. Journal of Reinforced Plastics and Composites 24, 1791–1807. DOI: 10.1177/0731684405052199.
14. LIN, H.J., AND LIN, J.J. 1996. *Nonlinear hydro elastic behavior of propellers using a finite-element method and lifting surface theory.* Journal of Marine Science and Technology 1, 114–124. DOI: 10.1007/BF02391167.
15. MALJAARS, P., BRONSWIJK, L., WINDT, J., GRASSO, N., AND KAMINSKI, M. 2018. *Experimental Validation of Fluid – Structure Interaction Computations of Flexible Composite Propellers in Open Water Conditions Using BEM-FEM and RANS-FEM Methods*. Journal of

Marine Science and Technology 6, 1–23. DOI:10.3390/jmse6020051.
16. MOURITZ, A.P., GELLERT, E., BURCHILL, P., AND CHALLIS, K., 2001. *Review of advanced composite structures for naval ships and submarines.* Composite Structures 53, 21–41.
17. OOSTERVELD, W.P.A. VAN L.D. VAN M.W.C.1969. *The Wageningen B-Screw Series*. New York.
18. OOSTERVELD, M.W.C., AND VAN OOSSANEN, P. 1975. *Further Computer-Analysed Data of the Wageningen B-Screw Series*.. International Shipbuilding Progress 22, 251–262.
19. SANGHO HAN, HYOUNGSUK LEE, MIN CHURL SONG, B.J.C. 2015. *Investigation of hydro-elastic performance of marine propellers using fluid-structure interaction analysis,* ASME 2015 International Mechanical Engineering Congress and Exposition. IMECE2015, Houston, Texas, pp. 1–9. DOI: /10.1115/IMECE2015-51089
20. SUBRAMANIAN V.A, VIJAYAKUMAR R, 2006. *"An inverse design approach for minimising wake at propeller plane using CFD"* Ocean Engineering, Vol 33, Issue 2, Pages 119-136
21. TROOST L. 1938. *Open water test series with modern propeller forms.* Trans. NECIES ;54.
22. TROOST L. 1938. *Open water test series with modern propeller forms.* II. Three bladed propellers. Trans. NECIES.
23. TROOST L. 1938. *Open water test series with modern propeller forms.* III. Two bladed and five bladed propeller Extension of the three and four bladed B-series. Trans. NECIES. 67.
24. YOUNG, Y.L. 2007. *Hydro elastic behavior of flexible composite propellers in wake inflow.* 16th international conference on composite materials. Japan Society for Composite Materials, Kyoto, Japan.
25. YOUNG, Y.L. 2008. *Fluid-structure interaction analysis of flexible composite marine propellers.* Journal of Fluids and Structures 24, 799–818. DOI: 10.1016/j.jfluid structs.2007.12.010.
26. YOUNG, Y.L, MOTLEY, M.R., AND BARBER, R. 2017. *Adaptive Composite Marine Propulsors and Turbines : Progress and Challenges.* Applied Mechanics Reviews 68, 1–34. DOI: 10.1115/1.4034659